CHEMISTRY OF MATERIALS

ARTICLE

pubs.acs.org/cm

Electrodeposited 3D Tungsten Photonic Crystals with Enhanced Thermal Stability

Kevin A. Arpin, Mark D. Losego, and Paul V. Braun*

Department of Materials Science and Engineering, Frederick Seitz Materials Research Laboratory, Beckman Institute, University of Illinois at Urbana−Champaign, Urbana, Illinois 61801, United States

ABSTRACT: Tungsten inverse opal photonic crystals were fabricated using a template directed electrodeposition method. The electrodeposition was accomplished using a molten salt solution at elevated temperatures. Following template removal, the tungsten inverse opals were conformally coated with hafnia or alumina via atomic layer deposition. This surface passivation layer increased the thermal stability of the tungsten microarchitectures by limiting surface diffusion. Alumina protected tungsten inverse opals were thermally stable up to 1000 °C for at least 12 h in forming gas (5% H_2 in Ar). Hafnia protected inverse opals were thermally stable up to 1400 °C for at least 12 h in forming gas. We expect that this surface passivation technique can also be implemented to increase the thermal stability of other refractory metal microarchitectures. The demonstrated thermal stability is an important property for the realization of metallic photonic crystals as narrow band emitters for thermophotovoltaics.

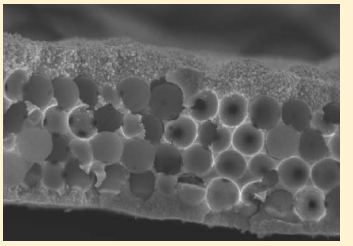

KEYWORDS: thermophotovoltaics, tungsten inverse opal, electrodeposition

INTRODUCTION

Photonic band gaps can emerge when materials are periodically organized with characteristic dimensions on the order of the wavelength of light. Such materials are commonly known as photonic crystals.[1] Proposed applications for photonic crystals include a wide range of functional optical devices including low-loss optical fibers,[2] three-dimensional waveguides,[3,4] zero-threshold lasers,[5] sensors,[6] and enhanced efficiency solar energy converters.[7,8] Periodic micro/nanoarchitectures with metallic components are especially interesting because they interact very strongly with light,[9] resulting in unique optical,[10] plasmonic,[11] and thermal emission properties.[12,13]

Solar thermophotovoltaic (sTPV) energy harvesting offers an attractive opportunity to achieve ultrahigh efficiency solar energy harvesting by effectively compressing the broad solar spectrum into a narrow band of energies, which can then be efficiently absorbed by a solar cell.[14−16] For maximum efficiency, electromagnetic radiation arriving at the solar cell should be concentrated at an energy just above the band gap energy of the solar cell. In this configuration, sub-band gap photons are not wasted and excess energy due to thermalization of high-energy photons is minimized, resulting in the high overall efficiency. Several materials/designs have been proposed to achieve narrow band emission, including rare earth doped materials, plasmas, optical filtration systems, and metallic photonic crystals.[17]

Metallic photonic crystals are particularly strong candidates to generate narrow band emission for sTPV energy harvesting systems.[13,18] Previous studies demonstrated that metallic photonic crystals could exhibit modified thermal emission as a direct result of the modulation of the optical density of states by their multidimensional periodic structure. For a blackbody in thermal equilibrium, Kirchoff's law tells us that emittance ≈ absorptance = 1 − reflectance. Thus, we can expect thermal emission to be greatly suppressed within the photonic band gap of a metallic photonic crystal and emission (absorption) to be enhanced at the photonic band gap edges.

Fleming et al. reported modified thermal emission due to the photonic bad gap of a lithographically prepared tungsten woodpile photonic crystal.[13] The woodpile fabrication is, however, complex. Thus, it is desirable to use a large area, low cost self-assembly process to fabricate metallic photonic crystals. On the basis of experimental studies with Ni inverse opals[18] and simulations of tungsten inverse opals,[19] we expect that a properly designed tungsten inverse opal photonic crystal could modulate thermal emission. Both control of surface termination and 3D filling fraction are important to ensure that light penetrates the 3D architecture and probes the photonic band structure. The concept of using a self-assembled opal template to fabricate tungsten inverse opals via CVD or solution-based inversion processes has been explored by a number of groups.[20−22] A significant problem with these inverse opal structures, however, is that they suffer from severe sintering and grain growth at elevated temperatures (beginning at 800 °C) resulting in the loss of the 3D periodicity and thus, the photonic band structure. Stein et al. published a notable exception, demonstrating thermal stability of a thin tungsten coating on a carbon scaffold up to 1000 °C for 5 h.[23]

Thermal stability at temperatures of 1000 °C or, preferably, greater, for extended times, is a key requirement for a sTPV emitter. In accordance with the Stefan−Boltzmann equation, the radiated power from a blackbody source will increase proportionally to the fourth power of the temperature of the emitter.[17] Various models suggest the overall energy conversion efficiency of a sTPV device will increase with increasing emitter temperatures up to possibly

Received: July 11, 2011
Revised: October 4, 2011
Published: October 18, 2011

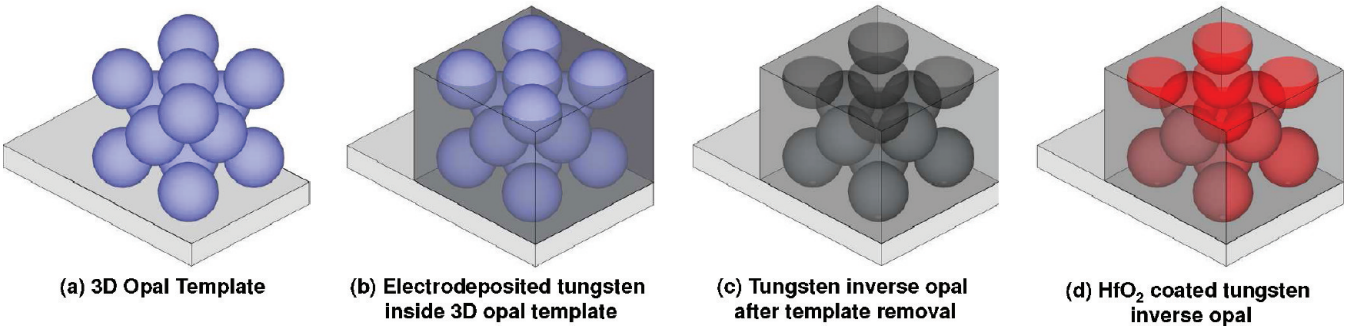

Figure 1. 3D template directed electrodeposition procedure. (a) Silica opals are grown on tungsten foils. (b) Tungsten is electrodeposited inside the 3D template. (c) Tungsten inverse opals are obtained after template removal by HF etching. (d) The tungsten inverse opals are coated with HfO_2 or Al_2O_3 by ALD to impart thermal stability.

60%, for an emitter temperature in the range of 1000−2000 °C[14,15,17,24] Fabricating such a *thermally stable* metallic photonic crystal to achieve narrow band emission using bottom up synthetic procedures, however, remains an unsolved challenge.

Here, we explore the fabrication of thermally stable 3D tungsten photonic crystals by electrodeposition through a 3D colloidal crystal template. One notable advantage of an electrodeposition approach is that it is a bottom up inversion technique that has the potential to yield dense deposits.[25] During electrodeposition, all void space is filled, leaving no pores, unlike gas phase deposition techniques, where pores are always generated due to "pinch off". We enhance the thermal stability of the electrodeposited tungsten inverse opals using the atomic layer deposition (ALD) of a conformal hafnia or alumina surface passivation layer.

EXPERIMENTAL SECTION

Figure 1 outlines the tungsten inverse opal fabrication procedure. A silica opal was used as a 3D template to direct the tungsten electrodeposition. The silica colloids were made using the well-known Stöber method,[26] and the opals were assembled by vertical deposition.[27] Before electrodeposition, the opals were coated with 10 nm of HfO_2 by ALD, which served to prevent lift-off from the tungsten substrate and preserve the 3D order during electrodeposition. Hafnia was deposited using a Savannah ALD system from Cambridge Nanotech. Following the tungsten electrodeposition, the 3D silica/hafnia template was removed by HF etching (5% HF in 1:1 water−ethanol solution). Note: HF is extremely toxic and should be handled with appropriate personal protection and inside a fume hood. Figure 2 shows a fracture cross section of the as-deposited tungsten before template removal and a top view of the tungsten inverse opal after template removal. Finally, 15 nm of hafnia (or alumina) was conformally coated on the tungsten inverse opal by ALD. The thickness of the coating was measured by ellipsometry. This coating provided the observed enhanced thermal stability.

Tungsten is not straightforward to electrodeposit because it has a high reduction potential. Electrodeposition must be done using a molten salt solution at elevated temperatures.[28] Our deposition conditions were based on reports of relatively low temperature electrodeposition of tungsten in a $ZnCl_2$−NaCl−KCl eutectic mixture (0.6:0.2:0.2 mol fraction).[29] The tungsten ion source was WO_3, and KF was added to increase the solubility of WO_3. Investigations into the melt composition show that WO_3 forms ionic complexes that can be reduced at the cathode (eq 1).[30]

$$WO_3F^- + 6e^- \rightarrow W + 3O_2^- + F^- \quad (1)$$

Free fluorine ions, however, etch the template materials (silica and hafnia). The minimum amount of KF required to solvate 0.29 mol % WO_3 while not causing etching was determined experimentally to be 1.2 mol % KF.

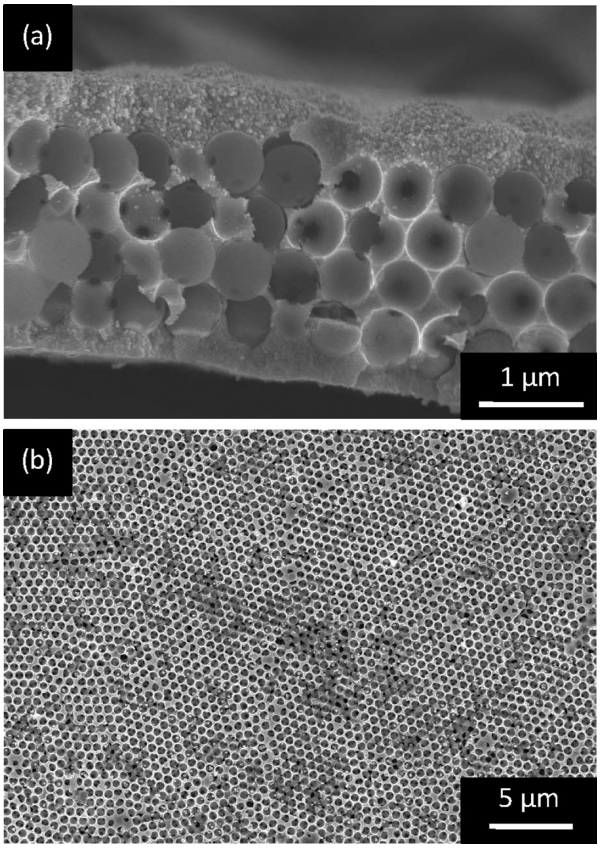

Figure 2. Scanning electron micrographs of a (a) fracture cross section after tungsten electrodeposition inside the 3D template and (b) the top surface of tungsten inverse opal after template removal by HF etching.

Tungsten electrodeposition was performed using a three-electrode cell consisting of a tungsten working electrode (cathode), a glassy carbon counter electrode, and a zinc reference electrode. All depositions were performed on a hot plate, at 425 °C, in a glovebox under an argon atmosphere. An initial pulsed deposition was used to provide uniform nucleation and growth. The pulsed deposition consisted of half-second on/off pulses at 50 and 200 mV, respectively. This cycle was repeated 1000 times before proceeding with a 50 mV constant potential electrodeposition until the 3D template was completely filled with tungsten.

The electrodeposited tungsten was imaged using a Hitachi S4800 high-resolution field emission scanning electron microscope. Elemental analysis was performed using an Oxford Instruments ISIS EDS X-ray

dx.doi.org/10.1021/cm2019789 |*Chem. Mater.* 2011, 23, 4783–4788

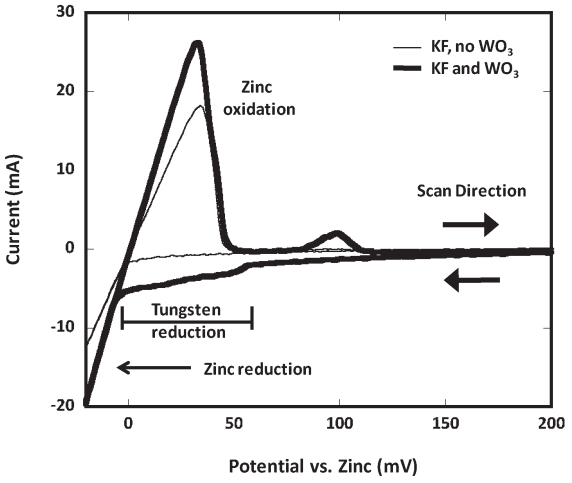

Figure 3. Cyclic voltammograms performed before (thin line) and after (thick line) the addition of the tungsten precursor (WO_3) at 425 °C under an inert atmosphere. Voltages reported were measured with respect to a zinc reference electrode. A cathodic current corresponding to tungsten electrodeposition was observed after the addition of WO_3. Tungsten electrodeposition was expected for voltages below 60 mV but above the potential corresponding to zinc electrodeposition (10 mV).

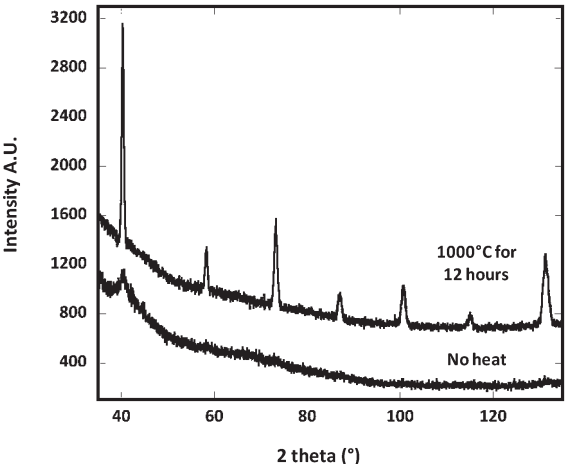

Figure 4. X-ray diffraction pattern of electrodeposited tungsten before and after heating to 1000 °C for 12 h in forming gas.

microanalysis system. X-ray diffraction analysis was performed using a Philips X'pert MRD system with Cu Kα radiation. Ellipsometry was performed using a Gaertner L116C, fixed angle, single wavelength, 632 nm. All thermal testing was done using a tube furnace. Forming gas (5% H_2 in Ar) was flowed over the samples during thermal treatment.

RESULTS AND DISCUSSION

Tungsten Electrodeposition. Potentiostatic electrodeposition was used to obtain the tungsten inverse opals. The ideal deposition voltage was determined experimentally using cyclic voltammetry (Figure 3). During cyclic voltammetry, the current at the cathode (tungsten foil) was measured as the potential was decreased from 200 to −10 mV and then increased from −10 back to 200 mV (see arrows in Figure 3). Prior to the addition of the tungsten precursor, only zinc electrodeposition (reduction) was observed starting at 10 mV (Figure 3, thin line). After the addition of the tungsten precursor, both zinc and tungsten electrodeposition (reduction) was observed (Figure 3, thick line). As the potential was decreased with the WO_3 precursor present in solution, a cathodic current was observed starting at ∼60 mV corresponding to tungsten electrodeposition. As the voltage decreased further, zinc electrodeposition was observed starting at ∼10 mV. Thus, we expected to observe tungsten electrodeposition in the range 10−60 mV. The quality of the deposited tungsten was strongly affected by the potential and current density. Void-free, pure, and fine-grained tungsten was observed at 50 mV (∼1 mA/cm^2). The as-deposited tungsten was largely amorphous, with perhaps some nanograined polycrystalline regions as determined by X-ray diffraction (Figure 4). X-ray diffraction analysis after heating at 1000 °C for 12 h in forming gas, indicates the tungsten was crystalline and in the alpha phase. The deposited material was pure tungsten, as determined by energy dispersive X-ray spectroscopy.

Thermally Stable Tungsten Inverse Opals. The physical properties of nanostructured materials can vary greatly from what is observed in the bulk. At reduced length scales, increased surface-to-volume ratios mean increasing numbers of atoms populate surface and interfacial sites. The thermal stability in such structures can therefore be dominated by the surface.[31] The promise of refractory metals for thermally stable nanostructures has not yet been fully realized because of sintering, grain growth, grain grooving, melting, and evaporation at elevated temperatures. You et al. demonstrated increased thermal stability of polycrystalline tungsten nanowires using a carbon shell.[32] The carbon shell stopped nanowire deformation during Joule heating, presumably by limiting surface diffusion. We previously demonstrated that an alumina passivation layer deposited by ALD improved the thermal stability of 3D Ni inverse opals by approximately 200 °C.[18] Without a protective coating, surface diffusion on the electrodeposited tungsten inverse opal drives grain coarsening resulting structural degradation. Our electrodeposited tungsten is fine grained and appears dense via SEM imaging; however, thermal treatment at 1000 °C in forming gas results in severe structural degradation due to sintering and grain growth (Figure 5), similar to what has been observed for 3D tungsten structures fabricated via chemical vapor deposition (CVD) or sol−gel methods.[20,22]

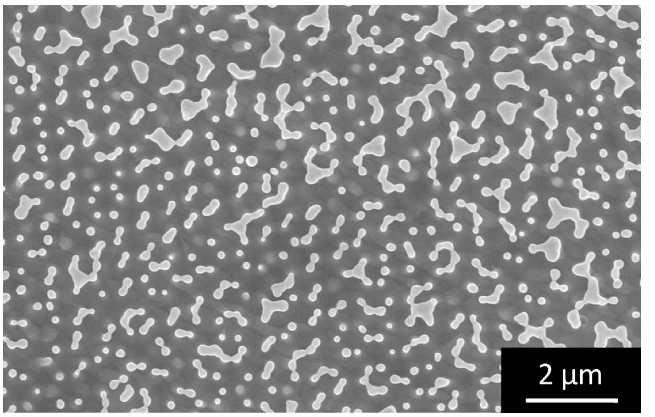

Figure 5. Scanning electron micrograph showing complete structural degradation after heating a tungsten inverse opal (not protected) to 1000 °C for 30 min in forming gas.

Hafnia and alumina are refractory materials that can be conformally coated within a 3D nanoarchitecture by ALD.

dx.doi.org/10.1021/cm2019789 |*Chem. Mater.* 2011, 23, 4783–4788

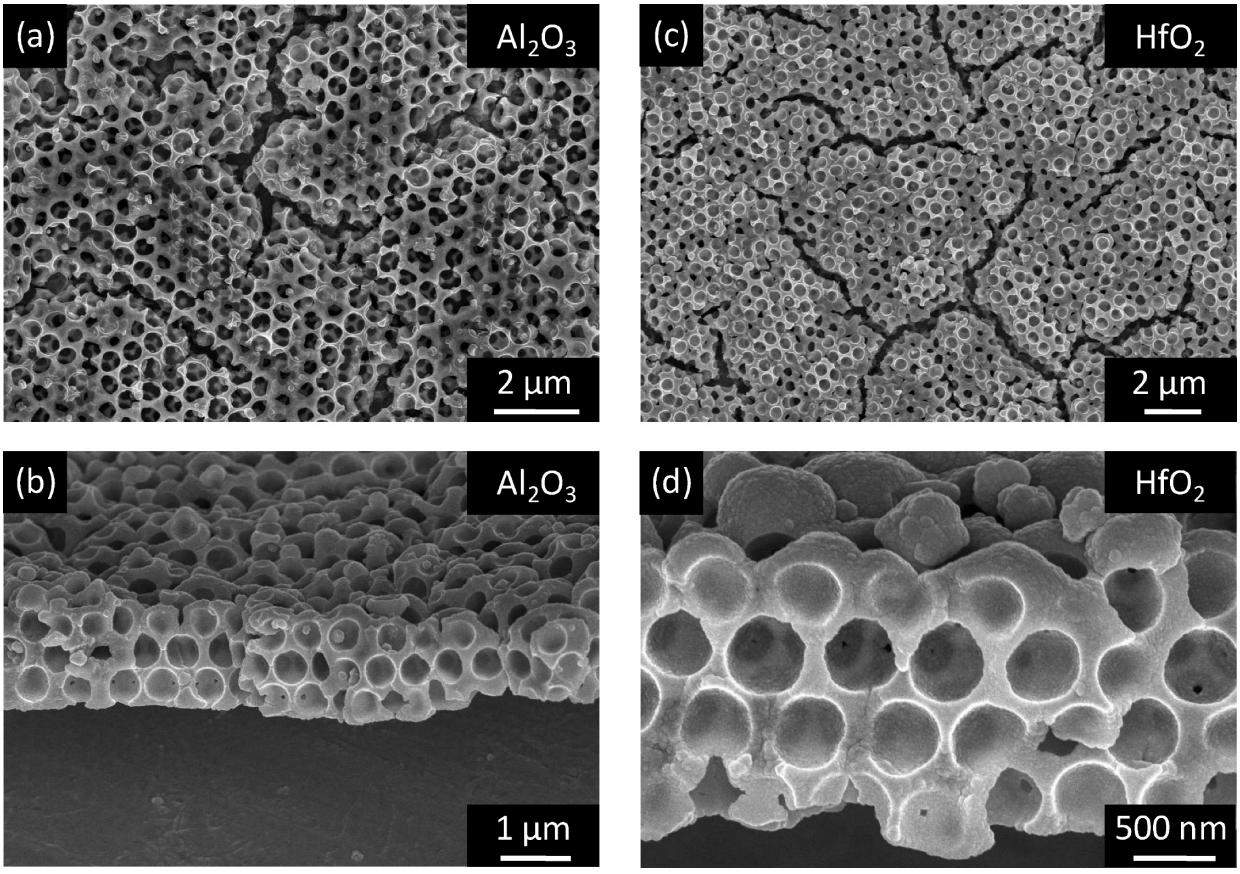

Figure 6. Scanning electron micrographs of tungsten inverse opals after heating to 1000 °C for 12 h. (a) Top surface and (b) fracture cross section of tungsten inverse opals protected with alumina. (c) Top surface and (d) fracture cross section of tungsten inverse opals protected with hafnia.

When applied as protective coatings on our tungsten inverse opals, the 3D structure was preserved at high temperatures for extended times, as evident using scanning electron microscopy. Figure 6 shows micrographs of tungsten inverse opals protected by alumina (parts a and b) and hafnia (parts c and d), after heating to 1000 °C for 12 h in forming gas. At this temperature, the effectiveness of hafnia and alumina as surface protective coatings were qualitatively similar. Perhaps the tungsten protected with alumina began densification at this temperature, as indicated by increased window sizes observed in Figure 6a. Densification and sintering were largely controlled and confined by the oxide shell, resulting in the preservation of the three-dimensional periodicity after thermal treatment. Presumably, the oxide passivation layer hindered surface diffusion, thus contributing to the prolonged structural integrity. However, densification during tungsten crystallization still resulted in internal stresses that gave rise to microscopic cracks with dimensions ~1 μm wide and ~1−10 μm long. This cracking behavior was not limited to our 3D structures. We observe similar cracking for nonstructured tungsten flat films electrodeposited under identical conditions (Figure 7), confirming that the cracks originate from the large volume shrinkage that occurs upon the crystallization of the electrodeposited film.

As previously described, the emitter temperature (T_E) is extremely important when considering the overall power production and energy conversion efficiency of a TPV system. The Stefan−Boltzman law tells us that the radiative power of a blackbody emitter, and thus the power available for electrical energy generation, increases as $\sim T_E^4$. Following the analysis by Chubb for an ideal system with an emitter temperature of 1000 °C, we can expect a TPV system's maximum electric power density to be ~0.1 W/cm^2 using a silicon solar cell. The maximum electric power density increases to ~1 W/cm^2 when the emitter temperature is increased to 1400 °C. Thus, a 400 °C increase in emitter operating temperature results in an order of magnitude increase in the power output of a TPV system. Note,

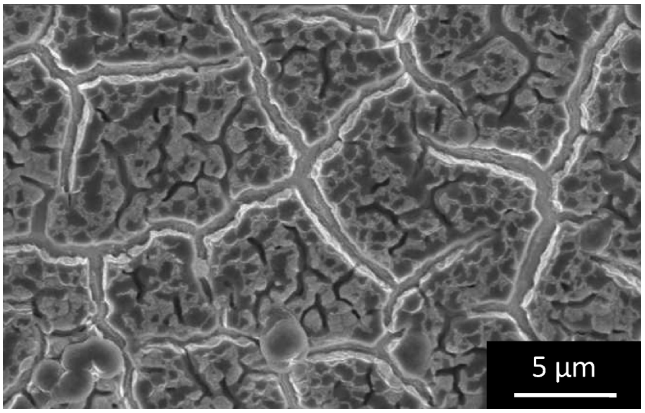

Figure 7. Scanning electron micrograph of a flat, nonstructured, electrodeposited tungsten film after heating to 1000 °C for 12 h in forming gas. Cracking is observed after heating as a result of internal stresses associated with densification.

dx.doi.org/10.1021/cm2019789 |*Chem. Mater.* 2011, 23, 4783–4788

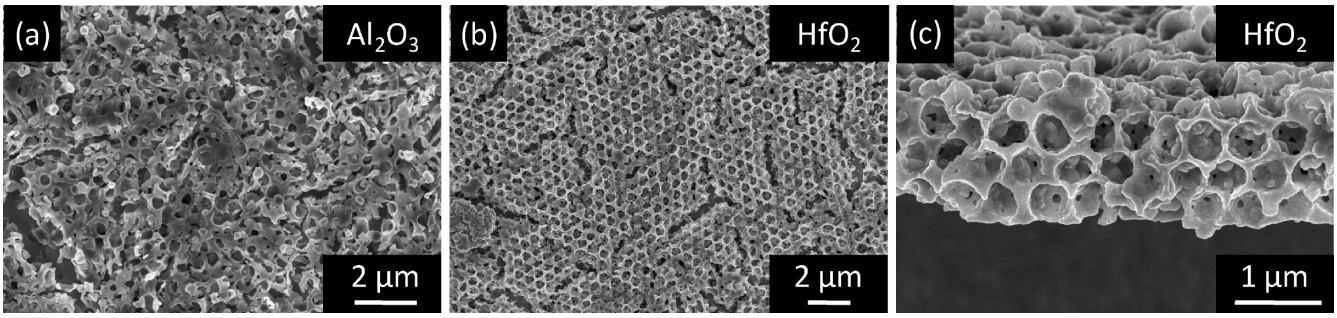

Figure 8. Scanning electron micrographs of tungsten inverse opals after heating to 1400 °C for 12 h. (a) Top surface of tungsten inverse opal protected with alumina. (b) Top surface and (c) fracture cross section of tungsten inverse opals protected with hafnia.

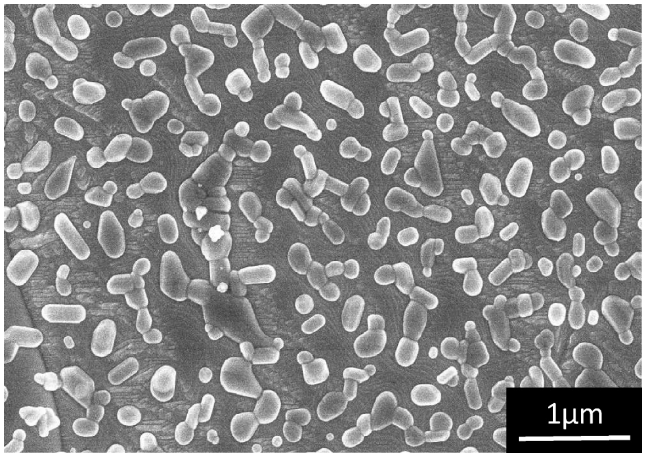

Figure 9. HfO_2 deposited on a flat tungsten foil substrate by ALD. Severe dewetting of the oxide occurs when heated to 1400 °C for 12 h. Dewetting was not observed at 1000 °C for 12 h.

the model assumes ideal photovoltaic cell, no losses from radiation heat transfer, and perfect vacuum between emitter and cell. The absolute values presented here for the electric power generation are theoretical values calculated and include many assumptions that ignore potential losses in real devices.

Because of the importance of temperature on sTPV performance, we have tested coated tungsten opals at higher temperatures. Figure 8 shows SEM micrographs of tungsten inverse opal structures protected with Al_2O_3 and HfO_2 after heating to 1400 °C for 12 h. At 1400 °C, the alumina coating did not sufficiently protect the 3D tungsten nanoarchitecture. After 12 h at 1400 °C in forming gas, the alumina passivated tungsten inverse opal collapsed and lost all 3D periodicity. The hafnia protected tungsten inverse opal largely survived the thermal treatment at 1400 °C. However, the structure does show evidence of increased grain growth and surface roughness compared to samples heated to 1000 °C.

The cause of the oxide passivation layer failure at 1400 °C is unknown. One possible answer could be that the oxide layer dewetts from tungsten at elevated temperatures. At 1000 °C, no dewetting of either oxide was observed. However, dewetting was observed after heating the ALD deposited oxide (alumina or hafnia) film on a flat tungsten foil for 12 h at 1400 °C in forming gas (Figure 9). This dewetting phenomenon was qualitatively similar for the hafnia and alumina films. When applied as a protective coating for 3D tungsten inverse opals, the oxide dewetting could be the cause of structural degradation.

CONCLUSIONS

Efficient narrow band emitters are essential for successful thermophotovoltaic energy conversion. Tungsten inverse opal photonic crystals are strong candidates for selective emitters; however, engineering thermally stable tungsten inverse opals remains an unsolved challenge. Here, via ALD, we implemented conformal refractory oxide coatings on tungsten inverse opal structures to impart increased thermal stability to the 3D structure. Alumina coatings increased stability up to 1000 °C while hafnia coatings stabilized the 3D structures up to 1400 °C. While volume-shrinkage upon crystallization limited complete 3D structural stability in our system, we think that this surface passivation technique is a universal approach to enhancing the thermal stability of 3D refractory metal structures. Further improvements in refractory metal deposition procedures combined with this surface passivation technique have the potential for producing thermally stable 3D architectures with large photonic band gaps and thermal emission modification properties necessary for TPV applications.

AUTHOR INFORMATION

Corresponding Author
*E-mail: pbraun@illinois.edu.

ACKNOWLEDGMENT

The authors would like to thank Chunjie Zhang, Dr. Ryan Haggerty, Dr. Masao Miyake, and Dr. Xindi Yu for useful discussions and experimental assistance. This work was supported by the Global Climate and Energy Project (GCEP) at Stanford University. This research was carried out in part in the Center for Microanalysis of Materials, UIUC, which is partially supported by the U.S. Department of Energy under Grant Nos. DE-FG02-07ER46453 and DE-FG02-07ER46471

REFERENCES

(1) Joannopoulos, J. D.; Johnson, S. G.; Winn, J. N.; Meade, R. D. *Photonic Crystals: Molding the Flow of Light*, 2nd ed.; Princeton University Press: Princeton, NJ, 2008.
(2) Russell, P. *Science* **2003**, *299* (5605), 358–362.
(3) Mekis, A.; Chen, J. C.; Kurland, I.; Fan, S. H.; Villeneuve, P. R.; Joannopoulos, J. D. *Phys. Rev. Lett.* **1996**, *77* (18), 3787–3790.
(4) Rinne, S. A.; Garcia-Santamaria, F.; Braun, P. V. *Nat. Photonics* **2008**, *2* (1), 52–56.
(5) Yablonovitch, E. *Phys. Rev. Lett.* **1987**, *58* (20), 2059–2062.

(6) Lee, Y. J.; Pruzinsky, S. A.; Braun, P. V. *Langmuir* **2004**, *20* (8), 3096–3106.
(7) Mihi, A.; Miguez, H. *J. Phys. Chem. B* **2005**, *109* (33), 15968–15976.
(8) Arpin, K. A.; Mihi, A.; Johnson, H. T.; Baca, A. J.; Rogers, J. A.; Lewis, J. A.; Braun, P. V. *Adv. Mater.* **2010**, *22* (10), 1084–1101.
(9) Moroz, A. *Phys. Rev. Lett.* **1999**, *83* (25), 5274–5277.
(10) Pendry, J. B. *Phys. Rev. Lett.* **2000**, *85* (18), 3966–3969.
(11) Ozbay, E. *Science* **2006**, *311* (5758), 189–193.
(12) Puscasu, I.; Pralle, M.; McNeal, M.; Daly, J.; Greenwald, A.; Johnson, E.; Biswas, R.; Ding, C. G. *J. Appl. Phys.* **2005**, *98* (1), 013531–1−6.
(13) Fleming, J. G.; Lin, S. Y.; El-Kady, I.; Biswas, R.; Ho, K. M. *Nature* **2002**, *417* (6884), 52–55.
(14) Harder, N. P.; Wurfel, P. *Semicond. Sci. Technol.* **2003**, *18* (5), S151–S157.
(15) Rephaeli, E.; Fan, S. H. *Optics Express* **2009**, *17* (17), 15145–15159.
(16) Swanson, R. M. *Proc. IEEE* **1979**, *67* (3), 446–447.
(17) Chubb, D. L. *Fundamentals of Thermophotovoltaic Energy Conversion*; Elsevier: Amsterdam, 2007.
(18) Yu, X. D.; Lee, Y. J.; Furstenberg, R.; White, J. O.; Braun, P. V. *Adv. Mater.* **2007**, *19* (13), 1689–1692.
(19) Han, S. E.; Stein, A.; Norris, D. J. *Phys. Rev. Lett.* **2007**, *99* (5), 053906−1–4.
(20) Chen, X.; Zhou, F.; Wang, J. X.; Li, M. Z.; Jiang, L.; Song, Y. L.; Li, Z. Y.; Zhu, D. B. *Appl. Phys. A: Mater. Sci. Process.* **2008**, *93* (2), 489–493.
(21) von Freymann, G.; John, S.; Schulz-Dobrick, M.; Vekris, E.; Tetreault, N.; Wong, S.; Kitaev, V.; Ozin, G. A. *Appl. Phys. Lett.* **2004**, *84* (2), 224–226.
(22) Denny, N. R.; Han, S. E.; Norris, D. J.; Stein, A. *Chem. Mater.* **2007**, *19* (18), 4563–4569.
(23) Nagpal, P. N.; Josephson, D. P.; Denny, N. R.; DeWilde, J.; Norris, D. J.; Stein, A. *J. Mater. Chem.* **2011**, *21*, 10836–10843.
(24) Baldasaro, P. F.; Raynolds, J. E.; Charache, G. W.; DePoy, D. M.; Ballinger, C. T.; Donovan, T.; Borrego, J. M. *J. Appl. Phys.* **2001**, *89* (6), 3319–3327.
(25) Lowenheim, F. A. *Modern Electroplating*, 3rd ed.; Wiley-Interscience: New York, 1974.
(26) Stober, W.; Fink, A.; Bohn, E. *J. Colloid Interface Sci.* **1968**, *26* (1), 62–69.
(27) Jiang, P.; Bertone, J. F.; Hwang, K. S.; Colvin, V. L. *Chem. Mater.* **1999**, *11* (8), 2132–2140.
(28) Simka, W.; Puszczyk, D.; Nawrat, G. *Electrochim. Acta* **2009**, *54* (23), 5307–5319.
(29) Nakajima, H.; Nohira, T.; Hagiwara, R.; Nitta, K.; Inazawa, S.; Okada, K. *Electrochim. Acta* **2007**, *53* (1), 24–27.
(30) Nitta, K.; Nohira, T.; Hagiwara, R.; Majima, M.; Inazawa, S. *Electrochim. Acta* **2010**, *55* (3), 1278–1281.
(31) Zhang, M.; Efremov, M. Y.; Schiettekatte, F.; Olson, E. A.; Kwan, A. T.; Lai, S. L.; Wisleder, T.; Greene, J. E.; Allen, L. H. *Phys. Rev. B* **2000**, *62* (15), 10548–10557.
(32) You, G. F.; Gong, H.; Thong, J. T. L. *Nanotechnology* **2010**, *21* (19), 195701.